IJC
International Journal of Cancer

Highly-expressed P2X7 receptor promotes growth and metastasis of human HOS/MNNG osteosarcoma cells *via* PI3K/Akt/GSK3β/β-catenin and mTOR/HIF1α/VEGF signaling

Yingchi Zhang, Hao Cheng, Wenkai Li, Hua Wu* and Yong Yang*

Department of Orthopedics, Tongji Hospital, Tongji Medical College, Huazhong University of Science and Technology, Wuhan, China

The P2X7 receptor, an ATP-gated ion channel, is critical for cancer cell growth, invasiveness, and angiogenesis. Previous studies indicate that P2X7 regulates osteoblast proliferation and osteodeposition and that high P2X7 expression has a pro-growth effect in osteosarcoma. However, how it functions in osteosarcoma cell growth and metastasis is not clear. Thus, we elucidated molecular mechanisms of P2X7-dependent positive regulation of osteosarcoma cell proliferation, invasion, migration, epithelial to mesenchymal transition (EMT), and angiogenesis using *in vitro* and *in vivo* models. We confirm that P2X7 is highly-expressed in human osteosarcoma tumor tissues and HOS/MNNG, MG63, U2OS, SW1353 and SAOS-2 cell lines. P2X7 receptor stimulation enhanced HOS/MNNG and SAOS-2 cell proliferation, migration and invasion; but knockdown of P2X7 expression or receptor inhibition had opposite effects. P2X7 positively regulated glycogen content, epithelial to mesenchymal transition and stemness of HOS/MNNG cells. P2X7 activation promoted PI3K/Akt/GSK3β/β-catenin and mTOR/HIF1α/VEGF signaling, thereby mediating pro-tumor effects of osteosarcoma cells. Consistent with data from *in vitro* experiments, systemic administration of P2X7 agonist induced tumor growth, metastasis and tumor-associated bone destruction in osteosarcoma-bearing nude mice, whereas a P2X7 antagonist reversed these effects. Thus, the P2X7 receptor participates in regulation of osteosarcoma growth and metastasis and we offer evidence that P2X7 may be a promising therapeutic target for treating osteosarcoma.

Introduction

Osteosarcoma is the most common bone cancer that predominantly affects children and adolescents and it is more likely to invade and create distant metastases.[1] Despite advances in multimodal treatments, frequent lung metastasis renders osteosarcoma refractory to standard therapies. The overall 5-year survival duration for osteosarcoma remains >60% for localized disease, but it is only 10–20% for metastatic disease.[2–4] Thus, better targeted therapeutics are needed to treat osteosarcoma to block tumor growth and stop metastasis.

Studies indicate that the tumor interstitium contains increased extracellular messenger ATP compared to healthy non-tumor counterparts. Di Virgilio's group reported relatively high extracellular ATP in tumor microenvironments experimentally induced tumors, whereas ATP was undetectable in tumor-free healthy tissues.[5] Tumor-derived ATP is hypothesized to modulate tumor growth, progression, and the immunosuppressive response, and is a major source of the immunosuppressant adenosine.[6,7] Extracellular ATP, mostly released in response to mechanical stimuli, is a natural ligand for P2Y metabotropic receptors and P2X ionotropic receptors. The P2X7 receptor is highly expressed in several malignancies including osteosarcoma and it is implicated in ATP-mediated cell growth, invasiveness, and angiogenesis.[8–12] The growth-promoting activity of P2X7 may be related to the

Key words: P2X7 receptor, osteosarcoma, PI3K/Akt signaling pathway, epithelial to mesenchymal transition, angiogenesis

Abbreviation: CSC: cancer stem cell; EMT: epithelial to mesenchymal transition; HIF: hypoxia inducible factor; mTOR: mammalian target of rapamycin; PI3K: phosphatidylinositol 3-kinase; TCF: T cell factor; VEGF: vascular endothecial growth factor

Additional Supporting Information may be found in the online version of this article.

Conflict of interest: The authors declare no conflict of interest.

*H.W. and Y.Y. contributed equally to this work and should be considered co-corresponding authors

Grant sponsor: National Natural Science Foundation of China; **Grant numbers:** 51537004, 51807078, 81301552

DOI: 10.1002/ijc.32207

History: Received 8 Nov 2017; Accepted 31 Jan 2019; Online 13 Feb 2019

Correspondence to: Hua Wu, Department of Orthopedics, Tongji Hospital, Tongji Medical College, Huazhong University of Science and Technology, Jiefang Avenue 1095, Wuhan 430030, China, Tel.: +86-027-83663023, Fax: +86-027-83663023, E-mail: wuhua360@aliyun.com; or Yong Yang, Department of Orthopedics, Tongji Hospital, Tongji Medical College, Huazhong University of Science and Technology, Jiefang Avenue 1095, Wuhan 430030, China, Tel.: +86-027-83663023, Fax: +86-027-83663023, E-mail: yangyong0127@hotmail.com

What's new?

The ATP-gated ion channel receptor P2X7 is increasingly recognized as a tumor-promoting factor. In this study, P2X7 was found to be overexpressed in human osteosarcoma tissues and cells, with its activation enhancing osteosarcoma cell proliferation, migration, and invasion. P2X7 activation further induced epithelial-mesenchymal transition (EMT), affected the stemness of osteosarcoma cells, and augmented angiogenesis. Experiments in mice showed that P2X7 also induces osteosarcoma-associated bone destruction. Opposing effects were observed upon P2X7 inhibition. P2X7 activity was influenced in part by PI3K/Akt/GSK3β/β-catenin and mTOR/HIF1α/VEGF signaling pathways. The data identify P2X7 as a target for the development of novel therapeutics against osteosarcoma.

proliferative advantage conferred to tumor cells especially under limited growth conditions, such as serum and glucose deprivation.[13–15] In addition, the P2X7 receptor promotes VEGF release to facilitate angiogenesis, cell invasion, and metastasis.[10,16,17] Numerous studies indicate that P2X7 is overexpressed in several cancers;[18–20] however, tumor-promoting pathways activated by P2X7 are not completely unraveled.

The phosphatidylinositol 3-kinase (PI3K)/Akt/mammalian target of rapamycin (mTOR) signaling pathway is known to contribute to many human cancers, including osteosarcoma.[21,22] Moreover, PI3K/Akt/mTOR signaling regulates tumor cell growth and angiogenesis by inducing expression of hypoxia inducible factor (HIF) 1α and VEGF.[23,24] S. Jeffrey's group recently reported that P2X7 receptor activation upregulated the canonical Wnt/β-catenin pathway *via* increased phosphorylation and inhibition of glycogen synthase kinase 3β (GSK3β) in osteoblast-like cells.[25,26] Inactivation of GSK3β evokes Wnt/β-catenin/T-cell factor (TCF) signaling and mediates Snail expression, which is responsible for epithelial to mesenchymal transition (EMT).[27,28] EMT is characterized by loss of the epithelial marker E-cadherin and increased expression of mesenchymal markers, such as Fibronectin and Vimentin.[29] Although the biological roles of these pathways in the initiation and progression of osteosarcoma are well established, efficacy for drugs interfering with downstream signaling molecules has been less than expected.[21,22] Therefore, identification of novel tumor-specific upstream pharmacological targets that modulate the PI3K/Akt/mTOR axis and/or canonical Wnt/β-catenin signaling may offer better treatment strategies for osteosarcoma.

To this end, we investigated the functional role of P2X7 in human osteosarcoma cells as a tumor promotor regulating proliferation, energy store, migration, invasion, EMT, metastasis, stemness and angiogenesis *in vitro* and *in vivo*. We also identified molecular mechanisms underlying P2X7 targeted signaling that involved the PI3K/Akt/GSK3β and Wnt/β-catenin pathways.

Materials and Methods

Reagents and antibodies

P2X7 agonist benzoyl ATP (BzATP), P2X7 antagonist A740003, and PI3K antagonist LY294002 were purchased from Sigma-Aldrich (St. Louis, MO). Akt, phospho (p)-Akt (Ser473), GSK3β, p-GSK3β (Ser9), mTOR, p-mTOR (Ser2448), HIF1α, β-catenin, TCF1 and lamin B1 rabbit monoclonal antibodies (Abs) were from Cell Signaling Technologies Inc. (Milan, Italy). P2X7, E-cadherin, fibronectin, vimentin, Snail, ALDH1A1, CD31, Ki67 and PCNA rabbit monoclonal Abs were purchased from Abcam (Cambridge, UK). CD133 antibody was from Miltenyi Biotec (Teterow, Germany).

Human osteosarcoma tissue collection and immunohistochemistry

A tissue array, containing samples from 2 normal bones and 10 stage IV osteosarcomas, was screened for P2X7 expression using immunohistochemistry. Specimens included samples from 7 male and 3 female patients with osteoblastic and chondroblastic osteosarcoma (11–50 years-of-age). Normal bone samples were obtained from patients undergoing hip replacement for transcervical fracture. All patients offered informed consent.

Cell culture

Human bone marrow mesenchymal stem cells (h-BMSCs), and HOS/MNNG, MG63, U2OS, SW1353, SAOS-2 osteosarcoma cell lines were purchased from the Cell Bank of Chinese Academy of Sciences (Shanghai, China) in September 2015. All cell lines were maintained in expansion medium consisting of DMEM/F12 supplemented with 10% FBS and 100 U/mL penicillin–streptomycin at 37°C and 5% CO_2. All cell lines were tested by Cell Bank of Chinese Academy of Sciences. All cell lines of passage 3–5 were used in following experiments.

AO/EB dual staining

For measurement of plasma membrane permeabilization, HOS/MNNG cells, with or without A740003 (5 μM) pretreated for 30 min, were then incubated with BzATP (0, 25, 125 or 250 μM) for 30 min. Afterwards, the HOS/MNNG cells were washed with PBS and stained with Aridine Orange (AO) and Ethidium Bromide (EB). Fluorescence emissions were visualized by a fluorescent microscopy. Relative EB fluorescence intensities were measured by a fluorescent plate reader. Fluorescence emission was measured at an excitation/emission wavelength of 360/580 nm.

Fluo 3-AM staining

For measurement of intracellular Ca^{2+}, HOS/MNNG cells were incubated with 5 μM Fluo 3-AM in glass-bottom dishes for 45 min at 37°C and washed three times with serum-free DMEM without phenol red, meanwhile the a part of cells were pretreated

with 5 μM A740003. Thereafter, the cells were incubated with BzATP (0, 25, 125 or 250 μM) for 1 min. The detection of intracellular Ca^{2+} was determined in Fluo 3-AM fluorescence by a fluorescent microscope. Relative Fluo 3-AM fluorescence intensities were measured by a fluorescent plate reader. Excitation and emission wavelength were 506 and 526 nm, respectively.

Lentiviral infection

Lentiviral vectors carrying short hairpin RNA (shRNA) targeting human P2X7 receptor (GV118) and the corresponding non-target control vector were obtained from GeneChem (Shanghai, China). The following target siRNA sequences of human P2X7 receptor were used: P2X7-RNAi GTGGCTTCAAGAGTCCTTA and non-targeting control TTCTCCGAACGTGTCACGT. HOS /MNNG and SAOS-2 cells (5×10^5 cells/well) were infected with lentivirus carrying shRNA with a multiplicity of infection (MOI) of 10 in the presence of 5 μg/mL polybrene (GeneChem, Shanghai, China) for 48 h at 37°C and 5% CO_2. Stable clones expressed green fluorescent protein and were selected with flow cytometry.

RNA extraction and qRT-PCR

Total RNA was extracted using Trizol reagent according to the manufacturer's instructions. RNA was quantified spectroscopically, and 3 μg RNA was reverse transcribed using an EasyScript First-Strand cDNA Synthesis Super Mix kit (TransGen Biotech, Beijing, China). Human P2X7, E-cadherin, fibronectin, vimentin, snail and GAPDH mRNA listed in Supporting Information Table S1 were quantified with quantitative real-time PCR. Bio-Rad myiQ2 Sequence Detection System (Bio-Rad, Hercules, CA) and TransStart Eco Green qPCR Super Mix (TransGen Biotech, Beijing, China) were used according to the manufacturer's protocol. Cycle conditions were as follows: 95°C for 30 s, 40 cycles at 95°C for 5 s, and 60°C for 35 s. Relative gene expression was assayed by normalizing with GAPDH using the $2^{-\Delta\Delta Ct}$ method.

Western blot

Cytoplasmic and nuclear protein was extracted using a Nuclear and Cytoplasmic Protein Extraction Kit (Beyotime) according to the manufacturer's protocol. Protein was measured using a BCA protein assay kit (Applygen, Beijing, China).

Equivalent amounts of protein were separated with 10% SDS-PAGE, and then transferred onto PVDF membranes. Membranes were blocked for 1 h at room temperature with 5% BSA in 1× TBST (0.1% Tween-20). Following incubation, membranes were probed with P2X7, Akt, p-Akt, GSK3β, p-GSK3β, E-cadherin, Fibronectin, Vimentin, Snail, ALDH1A1, β-catenin, mTOR, p-mTOR, HIF-1α, TCF-1, lamin B1 (all 1:1000) and GAPDH, β-actin (1:400) primary antibodies overnight at 4°C and with HRP-conjugated secondary antibodies (1:5000) at room temperature for 1 h. Membrane-bound proteins were visualized with ECL Western blot substrate and autoradiography. Band intensities were quantified with densitometric analysis (Image-Lab software, BioRad, Hercules, CA).

Immunofluorescence

Cells were fixed with 4% paraformaldehyde for 10 min, permeabilized in PBS containing 0.3% Triton X-100 for 15 min, and then blocked with 5% goat serum in PBS for 30 min. Cells were then incubated with P2X7, E-cadherin, fibronectin and β-catenin primary antibodies (1:200) at 4°C overnight, followed by 1 h incubation in FITC- or Cy3-labeled goat secondary antibodies (1:200) at room temperature. Nuclei were counterstained with DAPI (1:1). Stained samples were visualized using fluorescent microscopy (EVOS FL Auto Imaging System, Life technologies, Gaithersburg, MD).

Flow cytometry

Cancer stem cells (CSCs) were sorted from HOS/MNNG cells treated with 0, 5, 25 or 125 μmol/l BzATP or 5 μmol/l A740003 for 24 h and shRNA-transfected HOS/MNNG cells. Briefly, single-cell suspensions were washed in PBS, and stained with anti-CD133 antibody (FITC-conjugated; 1:100) for 30 min at 4°C. Stained cells were washed and resuspended with propidium iodide to exclude non-viable cells. CD133-positive cells were counted using a BD FACS flow cytometer (BD Biosciences, San Jose, CA).

Cell proliferation assay

The effects of BzATP and A740003 on cell proliferation after 24, 48, and 72 h of treatment were assessed using a Cell Counting Kit-8 (CCK-8) assay (Beyotime,) according to the manufacturer's protocol. Briefly, 10 μl CCK-8 solution was added to each well and incubated for 1.5 h in the dark, and absorbance (450 nm) was read using a microplate reader (Bio-Rad).

Wound healing assay

HOS/MNNG or SAOS-2 cells (1×10^6) in expansion medium were seeded in 6-well plates and cultured until 80% confluent. Cells were serum-starved overnight, and monolayers were mechanically disrupted using a sterile pipette tip to generate a linear wound. Subsequently, cells were washed in DMEM, and cultured in serum-free DMEM to determine the rate of wound closure.

Matrigel invasion assay

A matrigel invasion assay was performed in 24-well transwell plates. The upper and lower culture compartments were separated by polycarbonate filters with 8-μm pore diameter (Merck Millipore). Filters were pre-coated in sixfold diluted Matrigel (BD Biosciences, San Jose, CA). Equal numbers of HOS/MNNG or SAOS-2 cells (20,000 cells) in serum free DMEM were added to the upper chamber. The lower chamber was filled with DMEM medium containing 10% FBS for inducing cell migration, and plates were incubated for 12 h. Cells that traversed the membrane filter to the lower surface were fixed in 4% formalin for 5 min before staining with 0.1% crystal violet. Stained cells

were counted directly using a Nikon Eclipse TE2000-S microscope (Nikon, Tokyo, Japan).

Quantification of glycogen content

HOS/MNNG cells were maintained in serum-free medium for 24 h and treated with 125 μmol/l BzATP or 5 μmol/l A740003 at the same time. shRNA-transfected HOS/MNNG cells were maintained in serum-free medium for 24 h. Glycogen was measured using a periodic acid Schiff's (PAS) staining kit (Sigma) according to the manufacturer's protocol. Total and PAS positive cells were counted using Image Pro Plus 6.0 software.

VEGF quantification with ELISA

VEGF protein secreted into BzATP- or A740003-treated HOS/MNNG cell and shRNA-transfected HOS/MNNG cell culture supernatant was measured using a commercially available human VEGF ELISA kit (R&D Systems, Minneapolis, MN) according to the manufacturer's instructions.

Osteosarcoma tumor growth experiments

Female Balb/c-Nude mice (4–5 weeks old) were obtained from the Experimental Animal Center of Huazhong University of Science and Technology, Wuhan, China. All experimental procedures were approved by the Ethics and Animal Research Committee of Huazhong University of Science and Technology. HOS/MNNG cells were resuspended at 1×10^5/10 μl in PBS, and injected into the medullary cavity of the right tibia of mice ($n = 24$). When tumor volumes reached ~10–100 mm^3 (day 10 from cell injection) mice were divided into 4 groups ($n = 6$ mice/group), and treated with 200 μl (ip) of (1) placebo (PBS + 0.005% DMSO), (2) BzATP (0.25 mg/kg), (3) A740003 (0.025 mg/kg) or (4) BzATP (0.25 mg/kg) + A740003 (0.025 mg/kg) every day for 20 days. Tumor size was measured using a caliper every other day. Tumor volume was calculated using the following formula: volume = $\pi/6 \quad (w1 \times (w2)^2)$, where w1 = major diameter (mm) and w2 = minor diameter (mm) of the tumor. At the end of experiments, mice were sacrificed. Tumor and lung specimens were excised and washed in PBS, and stored at −80°C or fixed in Bouin's solution for immunohistochemical analysis.

Micro-computed X-ray tomography (μCT)

To determine presence of tumor-associated bone destruction in proximal tibia, a Scanco viva CT 40 (Scanco Medical AG, Bruttisellen, Switzerland) was used. Contiguous cross-sectional images were acquired at 70 kV, 114 mA, 300 ms integration, 500 projections per 1808 rotation, with a 12 mm isotropic voxel size. The bone tissue was segmented from soft tissue using a threshold of 270 per thousand (or 438.7 mgHA/cm3), a Gaussian noise filter of 0.8, and support of 2. Relative volume (BV/TV) of the tibiae [total bone (cortical + trabecular)] were quantified for each group and compared to the tibia of control rats.

Histological studies

Mice lung and tumor tissues were embedded in paraffin, and cut into 4-μm sections. Lung sections were stained with hematoxylin and eosin (H&E) to assess metastases in osteosarcoma-bearing mice. Immunohistochemical quantification of P2X7 in tissue arrays and Ki67 in tumor was done by rehydrating sections, which were then washed in TBS and blocked in TBS supplemented with 10% BSA for 1 h at room temperature. Sections were then incubated with primary antibodies diluted in TBS containing 3% BSA (1:100) for 1 h at room temperature. Slides were then washed twice in TBS containing 0.025% Triton X-100. Endogenous peroxidase activity was blocked by incubating slides in TBS/0.3% H_2O_2 solution for 20 min at room temperature. After several rinses in TBS, sections were incubated for 1 h at room temperature with HRP-conjugated antibody diluted in TBS/1% BSA (1:200). Tissue sections were washed twice in TBS, and peroxidase activity detected with Liquid DAB Substrate Chromogen System (Dako, Glostrup, Denmark). Nuclear counterstaining was performed using Mayer's hematoxylin.

Statistical analysis

All *in vitro* experiments were performed at least three times, and data are presented as means ± SD. For *in vivo* studies, tumor volumes are expressed as means ± SD. All quantified data represent an average of three independent experiments unless indicated otherwise. Error bars represent standard deviation of the mean. Statistical analyses were performed using SPSS software (version 19.0; SPSS Inc., Chicago, IL). Differences between two groups were assessed using student's t tests. Differences among three or more groups were evaluated by one-way ANOVA followed by the Tukey's post-hoc tests. Differences among multiple groups over multiple times were evaluated by two-way ANOVA followed by the Bonferroni's post-hoc tests. $p < 0.05$ was considered statistically significant.

Results

P2X7 is overexpressed in human osteosarcoma tissue and cell lines

A tissue array containing samples from 2 normal bones and 10 stage IV osteosarcomas was screened for P2X7 expression by immunohistochemistry. All osteosarcoma samples stained strongly positive for P2X7 protein while the normal bone tissue was weakly positive (Fig. 1*a*). P2X7 mRNA and protein expression were also upregulated in all 5 tested human osteosarcoma cell lines, namely HOS/MNNG, MG63, U2OS, SAOS-2 and SW1353, in comparison to human bone marrow mesenchymal stem cells (h-BMSCs). Among the five osteosarcoma cell lines, P2X7 expression was the highest in HOS/MNNG and the lowest in SAOS-2, so we chose these two cell lines as representative models to study the role of P2X7 in osteosarcoma growth and metastasis *in vitro*. (Figs. 1*b* and 1*c*). After downregulating P2X7 expression in HOS/MNNG and SAOS-2 cells, P2X7 mRNA and protein expression was reduced by 75% and 65% respectively compared to HOS/MNNG and SAOS-2 cells infected

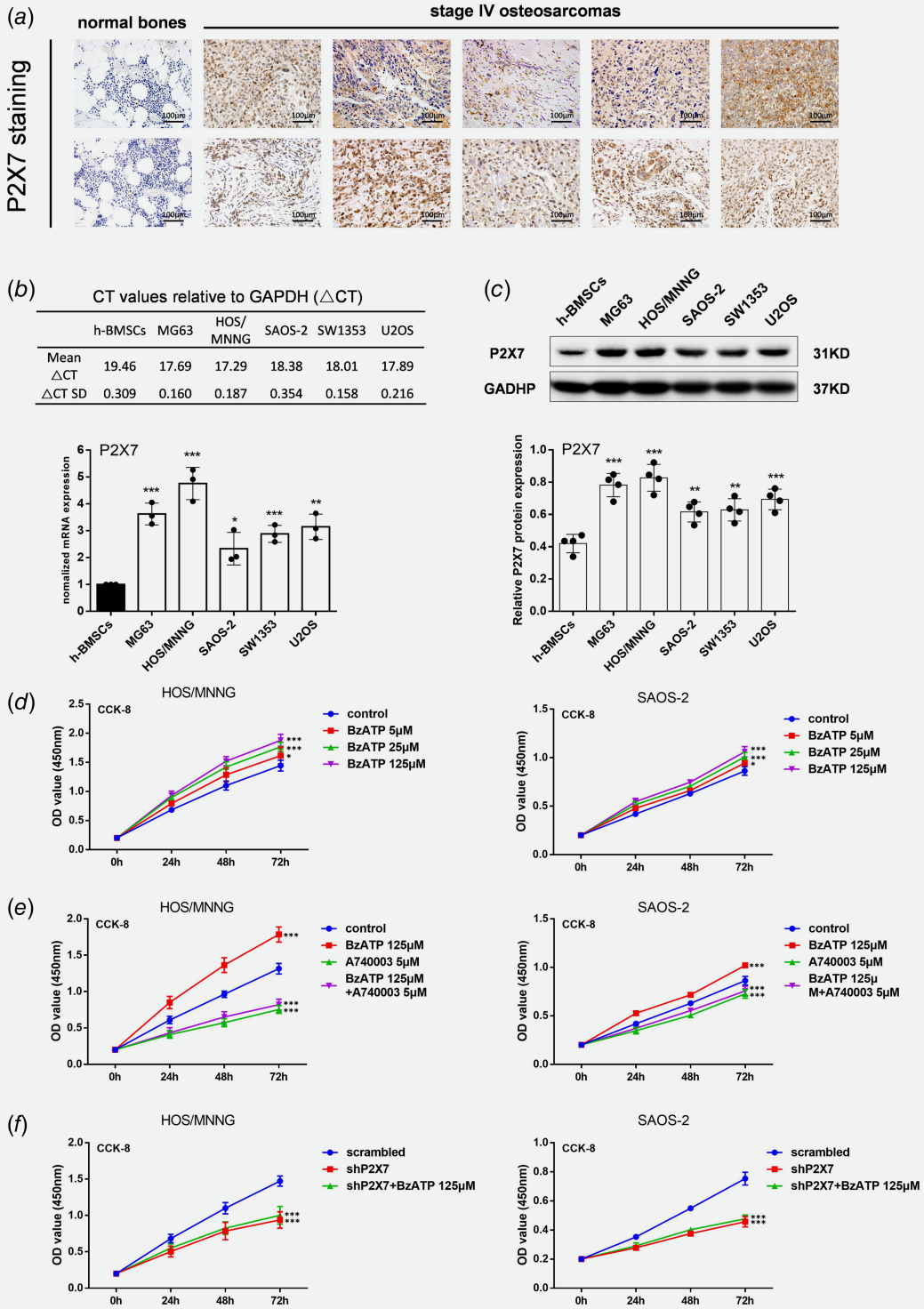

Figure 1. P2X7 is highly expressed in osteosarcoma and increases proliferation of HOS/MNNG and SAOS-2 cells. (*a*) Immunohistochemical staining for P2X7 in normal bones (n = 2) and stage IV osteosarcomas (n = 10). Specimens included samples from 7 male and 3 female patients with osteoblastic and chondroblastic osteosarcoma (11–50 years-of-age). Normal bone samples were obtained from patients undergoing hip replacement for transcervical fracture. Scale = 3 × 3 × 3 cm^3. Quantification of P2X7 (*b*) mRNA and (*c*) protein in human osteosarcoma cell lines, MG63, HOS/MNNG, SAOS2, SW1353 and U2OS, and human bone marrow mesenchymal stem cells (h-BMSC) as control. Relative gene or protein expression was assayed by normalizing with GAPDH. HOS/MNNG and SAOS-2 cell proliferation after 24, 48, and 72 h of treatment with (*d*) BzATP (5, 25 or 125 μM), (*e*) A740003 (5 μM) with or without BzATP (125 μM), and (*f*) lentiviral vectors with or without BzATP (125 μM) (n = 6). Proliferation rate was evaluated using CCK-8 assay. Data are means ± SD of 6 or 3 independent experiments. $^{***}p < 0.001$, $^{**}p < 0.01$, $^{*}p < 0.05$ *vs.* control. [Color figure can be viewed at wileyonlinelibrary.com]

with control vector (scrambled) (Supporting Information Fig. S1A-C). To test the pore and channel functionality of P2X7 in HOS/MNNG cells, AO/EB dual staining and Fluo-3-AM staining were used. After activating P2X7 by its specific agonist, BzATP, HOS/MNNG Cells exhibited increased plasma permeabilization and intracellular Ca^{2+}, which suggested that P2X7 is functional in HOS/MNNG cells (Supporting Information Fig. S2 A-B).

P2X7 increased proliferation, migration and invasion of HOS/MNNG and SAOS-2 cells

BzATP, a highly effective P2X7 receptor agonist, increased proliferation of HOS/MNNG and SAOS-2 cells compared to controls. The extent of proliferation increased from 15% to 35% when the BzATP concentration increased from 5 to 125 μM (Fig. 1*d*). Inhibiting the P2X7 receptor with A740003 (5 μM), a selective P2X7 antagonist, significantly reduced the effect of BzATP on HOS/MNNG and SAOS-2 cell proliferation by 50% and 40% (Fig. 1*e*). In addition, A740003 also reduced the basal proliferation of HOS/MNNG and SAOS-2 cells by 33% and 17%, respectively. P2X7 knockdown inhibited HOS/MNNG and SAOS-2 cell proliferation by 27% and 20% compared to scrambled control while BzATP treatment could not significantly increase proliferation of P2X7 knockdown cells. (Fig. 1*f*).

To examine whether migration could be regulated by P2X7 in osteosarcoma cell lines, wound-healing assay were used. HOS/MNNG and SAOS-2 cells treated with BzATP had more migration across wounds at 12 h compared to control. 5 to 125 μM BzATP increased HOS/MNNG cell migration by 35% to 171% and increased SAOS-2 cell migration by 65% to 250% (Fig. 2*a*). A740003 intensively lowered the effect of BzATP by more than 3 quarters and also decreased HOS/MNNG and SAOS-2 cell migration on its own (Fig. 2*e*). Figure 2*c* shows that the area covered by HOS/MNNG or SAOS-2 cells after shP2X7 with or without BzATP stimulating reduced by half at 12 h compared to scrambled control cells. We then measured the metastatic potential of the cells after P2X7 knockdown using Transwell invasion assays. Figure 2*d* shows that invading HOS/MNNG or SAOS-2 cells increased by 20% to 150% after 5 to 125 μM BzATP treatment compared to controls. In contrast, A740003 reduced pro-invasive effect of BzATP by 75% and also reduced the basal cell invasion by 30% (Fig. 2*e*). Additionally, infiltrating cells infected with shP2X7 were half less than scrambled infected cells, even in present of BzATP (Fig. 2*f*). Therefore, activated P2X7 receptors contribute to osteosarcoma cell proliferation, growth and invasiveness.

In addition, our results showed no significant differences between shP2X7 group and shP2X7 + A740003 group in all CCK-8, wound healing and Transwell invasion assays (Supporting Information Fig. S3 A-C).

P2X7 positively regulates EMT and stemness

To avoid repetitive and complex work, we chose one cell line, HOS/MNNG, to investigate the cancer-promoting mechanism of P2X7. EMT is required for tumor metastasis, which is characterized by loss of the epithelial marker E-cadherin, together with upregulated nuclear factor Snail and increased expression of mesenchymal markers, such as Fibronectin, and Vimentin.[30] To learn whether P2X7 regulates EMT, we measured E-cadherin, Fibronectin, Vimentin and Snail and confirmed a 12% to 40% decrease of E-cadherin mRNA and protein after 5 to 125 μM BzATP treatment. And also as expected, Snail, Vimentin, and Fibronectin increased 20%–100% at mRNA level and 20%–70% at protein level (Figs. 3*a* and 3*b*). In contrast, A740003 treatment downregulated Snail, Vimentin and Fibronectin mRNA and protein, and increased E-cadherin (Figs. 3*c* and 3*d*). Similar results were obtained in HOS/MNNG cells with P2X7 knockdown. shP2X7 twofold upregulated E-cadherin and inhibited other EMT markers by approximately 50% while BzATP could not reverse this effect, suggesting that P2X7 was involved in the regulation of EMT (Figs. 3*e* and 3*f*). Immunofluorescent data also confirmed these findings (Supporting Information Fig. S4A-D).

EMT is associated with malignant stem cell function,[30] and previous studies indicate that cancer stem cells (CSCs) are involved in tumor metastasis and relapse.[31–34] To determine whether P2X7 affected stemness of osteosarcoma cells, we sorted CSCs from osteosarcoma cell lines using flow cytometry and treated them with BzATP or A740003. 15% to 50% more $CD133^{high}$ CSCs were detected in 5 to 125 μM BzATP treated HOS/MNNG cells, but inhibition of P2X7 using an antagonist or shRNA decreased $CD133^{high}$ CSCs by 50%. (Fig. 3*g*) BzATP could not significantly increase $CD133^{high}$ CSCs in P2X7 inhibited cells (Figs. 3*h* and 3*i*; Supporting Information Fig. S5A-C). We validated these data with ALDH1 by Western blot and noted that ALDH1 protein increased in HOS/MNNG cells treated with BzATB (Fig. 3*j*); P2X7 inhibition decreased ALDH1 protein (Figs. 3*k* and 3*l*).

PI3K/Akt/GSK3β signaling participates in P2X7-dependent proliferation, migration, invasion and glycogen accumulation

To investigate the underlying mechanisms of P2X7-dependent proliferation, migration and invasion, PI3K/Akt/GSK3β progrowth signaling was assessed. Stimulation of HOS/MNNG cells with BzATP (5 μM to 125 μM) for 24 h resulted in a 1.3- to 2.3-fold increase of phosphorylated Akt and a 1.6- to 3.3-fold increase of phosphorylated GSK3β (Fig. 4*a*). In contrast, blocking P2X7 receptor with A740003 or shP2X7, in present of BzATP or not, significantly reduced the rate of Akt and GSK3β phosphorylation compared to control (Figs. 4*b*–4*c*).

Then, we use a PI3K blocking drug, LY294002, to clarify the connection between PI3K/Akt/GSK3β signaling and cell proliferation, migration and invasion. We treated HOS/MNNG cells with, respectively, A740003, LY294002 and A740003 + LY294002. All these 3 treatments suppress proliferation, migration and invasion to a similar degree (≈50%), whereas the joint treatment of A740003 and LY294002 did not cause an additional suppression (Figs. 4*d*–4*f*). Active GSK3β blocks glycogen

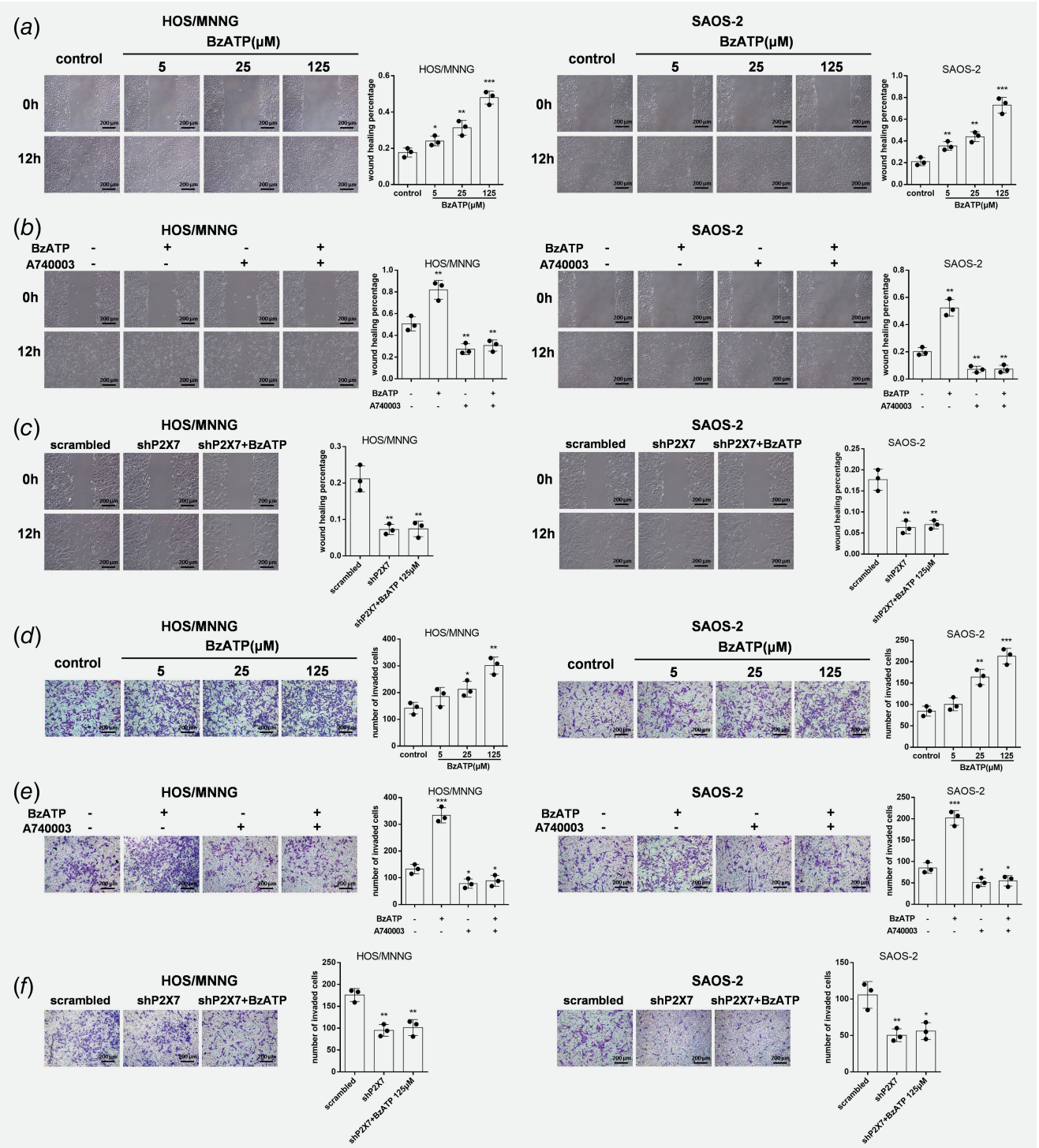

Figure 2. P2X7 increases migration and invasion of HOS/MNNG and SAOS-2 cells. Microscopic images of wound healing assay data for HOS/MNNG and SAOS-2 cells treated with (*a*) BzATP (5, 25 or 125 μM) or (*b*) A740003 (5 μM) with or without BzATP (125 μM) for 24 h, or (*c*) lentiviral vectors with or without BzATP (125 μM) (n = 3). Wound healing percentage was evaluated using Image Pro Plus 6.0 software. Microscopic images and Transwell assay data for invading HOS/MNNG and SAOS-2 cells ($\times 10^4$) treated with (*d*) BzATP (5, 25 or 125 μM), (*e*) A740003 (5 μM) with or without BzATP (125 μM) for 12 h, or (*f*) lentiviral vectors with or without BzATP (125 μM) (n = 3). Cells that traversed the membrane filter to the lower surface were stained with 0.1% crystal violet and counted using Image Pro Plus 6.0 software. Data are means ± SD of 6 or 3 independent experiments. $^{***}p < 0.001$, $^{**}p < 0.01$, $^{*}p < 0.05$ *vs.* control. [Color figure can be viewed at wileyonlinelibrary.com]

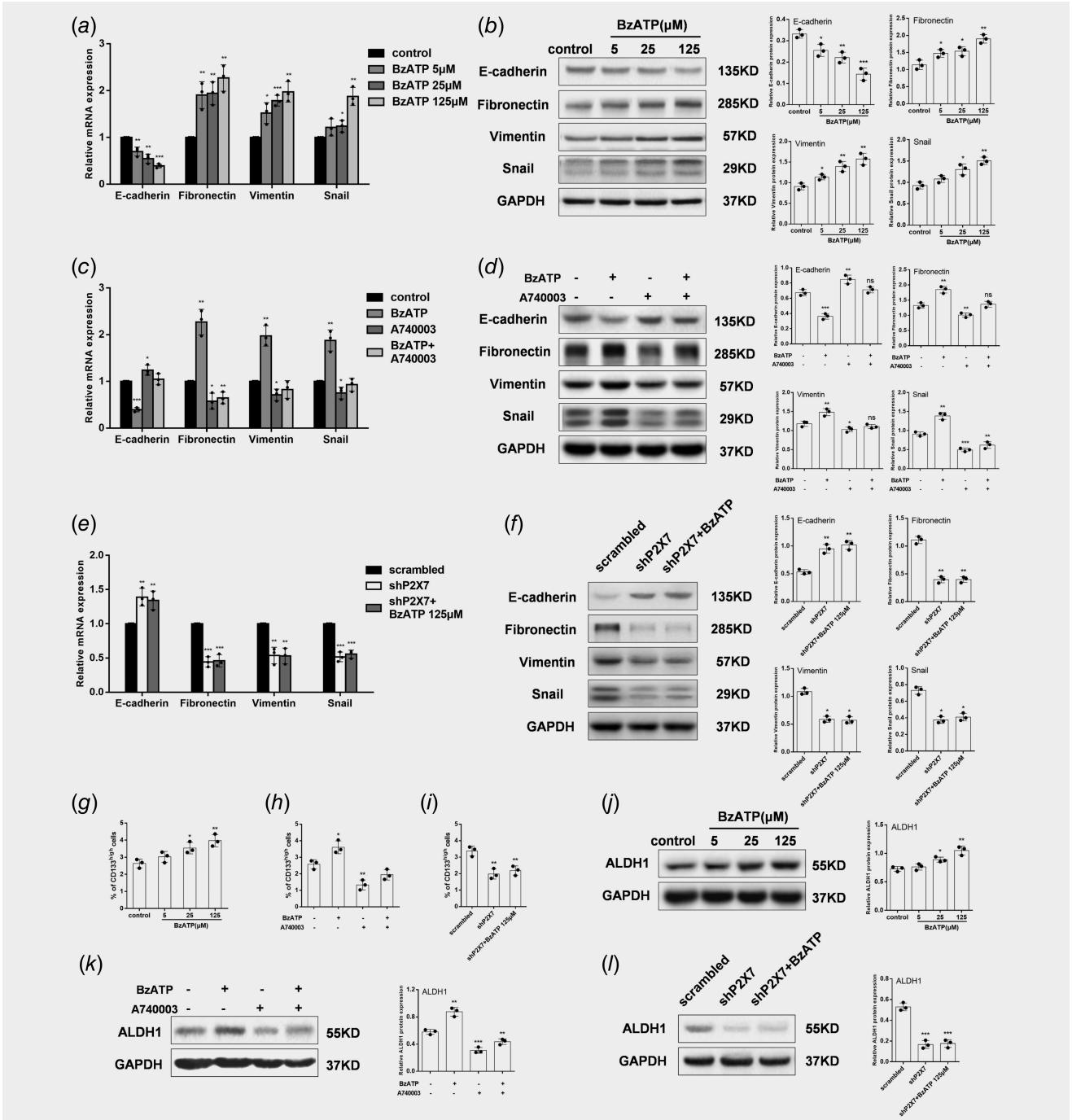

Figure 3. P2X7 positively regulates EMT and stemness. HOS/MNNG cells were treated with BzATP (5, 25 or 125 μM), A740003 (5 μM) or with or without BzATP (125 μM) for 24 h, or lentiviral vectors bearing scrambled or P2X7 shRNAs with or without BzATP (125 μM). E-cadherin, fibronectin, vimentin, and snail protein and mRNA quantified with Western blot or qRT-PCR, respectively. (*a*) mRNA and (*b*) protein of EMT in BzATP-treated (5, 25 or 125 μM for 24 h) HOS/MNNG cells. (*c*) mRNA and (*d*) protein in HOS/MNNG cells treated with BzATP (125 μM) or A740003 (5 μM) or both for 24 h. (*e*) mRNA and (*f*) protein of EMT markers in HOS/MNNG cells transfected with scrambled or shP2X7 lentiviral vectors or treated with shP2X7 and BzATP (125 μM). (*g*) $CD133^{high}$ cell population and (*j*) ALDH1 expression in HOS/MNNG cells treated with BzATP (5, 25 and 125 μM) for 24 h. (*h*) $CD133^{high}$ cell population and (*k*) ALDH1 expression in HOS/MNNG cells treated with BzATP (125 μM) or A740003 (5 μM) or both for 24 h. (*i*) $CD133^{high}$ cell population and (*l*) ALDH1 expression in HOS/MNNG cells transfected with scrambled or shP2X7 lentiviral vectors or treated with shP2X7 and BzATP (125 μM). Relative gene or protein expression was assayed by normalizing with GAPDH. CD133-positive cells were counted using a BD FACS flow cytometer. Data are means ± SD of 3 independent experiments. $^{***}p < 0.001$, $^{**}p < 0.01$, $^{*}p < 0.05$ *vs.* control.

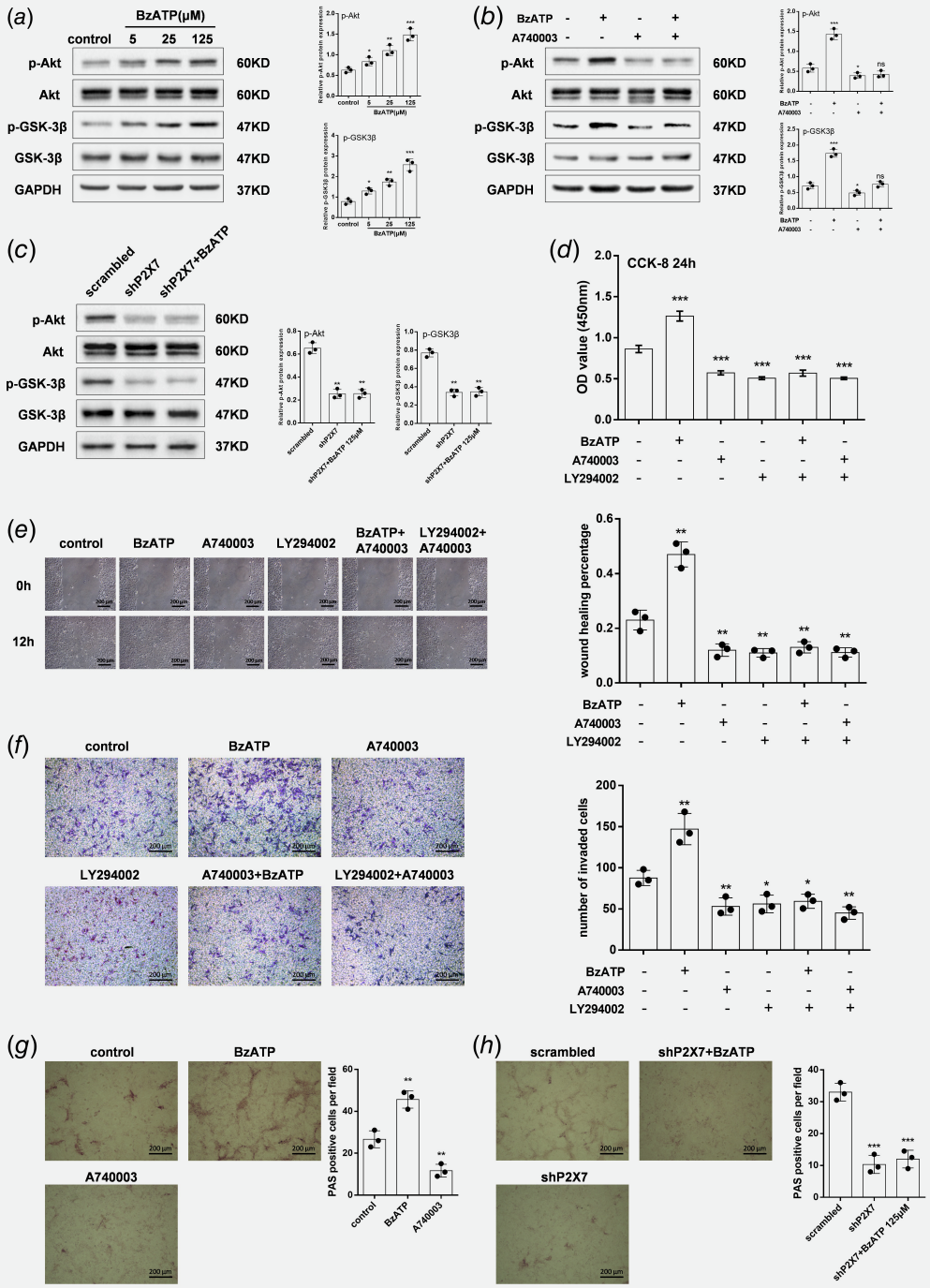

Figure 4. PI3K/Akt/GSK3β signaling participates in P2X7-dependent proliferation, migration, invasion and glycogen accumulation. Western blot of HOS/MNNG cells treated with (*a*) BzATP (5, 25 or 125 μM), (*b*) A740003 (5 μM) with or without BzATP (125 μM) for 12 h and (*c*) lentiviral vectors with or without BzATP (125 μM), and probed with total Akt, phosphorylated (p)-Akt (Ser473), total GSK3β, p-GSK3β (Ser9), and GAPDH antibodies. Representative results from 3 independent experiments are shown. (*d*) CCK-8 cell proliferation assay, (*e*) wound healing assay, and (*f*) Transwell invasion assay in HOS/MNNG treated with BzATP (125 μM), PI3K inhibitor LY294002 (20 μM), or A740003 (5 μM) for 12 h. Glycogen content measured with PAS staining in HOS/MNNG cells treated with (*g*) BzATP (125 μM) or A740003 (5 μM) for 24 h, or (*h*) lentiviral vectors with or without BzATP (125 μM). Relative protein expression was assayed by normalizing with GAPDH. Proliferation rate was evaluated using CCK-8 assay. Wound healing percentage was evaluated using Image Pro Plus 6.0 software. Cells that traversed the membrane filter to the lower surface were stained with 0.1% crystal violet and counted using Image Pro Plus 6.0 software. PAS positive cells were counted using Image Pro Plus 6.0 software. Data are means ± SD of 3 independent experiments. $^{***}p < 0.001$, $^{**}p < 0.01$, $^{*}p < 0.05$ *vs.* control. [Color figure can be viewed at wileyonlinelibrary.com]

synthase activity, depleting glycogen stores.[35] To confirm a link between P2X7 and GSK3β activity, we evaluated whether P2X7 influenced glycogen accumulation in osteosarcoma cells. HOS/MNNG cells were treated with 125 μM BzATP or 5 μM A740003 for 24 h, and glycogen was measured as shown in Figure 4*g*. BzATP treatment increased PAS-positive cells by 70% compared to control, and A740003 reduced glycogen accumulation by 50% in HOS/MNNG cells. PAS-positive cells in P2X7 knockdown groups, both in present of BzATP or not, had only about one third of that in scrambled control, confirming the link between P2X7 and GSK3β (Fig. 4*h*).

P2X7 activates Wnt/β-catenin signaling

The Wnt/β-catenin signaling pathway is necessary for the pathobiology and progression of osteosarcoma by inactivating GSK3β and increasing expression of nuclear factor Snail.[21] We observed increased GSK3β phosphorylation in osteosarcoma cells after P2X7 activation (Fig. 4*a*). We next investigated biological effects of P2X7-induced HOS/MNNG cell migration, invasion, EMT or stemness on the Wnt/β-catenin pathway by measuring downstream signaling molecules. 5 to 125 μM BzATP 1.7- to 2.7-fold increased mRNA of β-catenin and TCF-1, an endogenous substrate of GSK-3β (Fig. 5*a*), and augmented nuclear accumulation of β-catenin (1.7- to 2.2-fold) and TCF-1 (1.3- to 3.25-fold) (Figs. 5*d* and 5*g*). In contrast, inhibition of P2X7 with A740003 or shP2X7 decreased expression of β-catenin and TCF-1 by more than 50% (Figs. 5*b* and 5*c*), and reduced nuclear accumulation of β-catenin and TCF-1 by a similar degree of 40% (Figs. 5*e*–5*h*). BzATP treatment after P2X7 inhibitation could not significantly increase β-catenin and TCF-1 expression and enhance nuclear accumulation of β-catenin and TCF-1. So, P2X7 stimulates the Wnt signaling pathway, eventually leading to transcriptional activation of target genes.

P2X7 modulates mTOR/HIF1α/VEGF signaling

Angiogenesis is typical of human osteosarcoma, and inhibition of VEGF can reduce tumor angiogenesis and growth in an experimental osteosarcoma model *via* inactivation of the PI3K/Akt signaling pathway. Because the mTOR/HIF1α/VEGF axis is downstream of the PI3K/Akt pathway and involved in angiogenesis, we determined whether P2X7 receptor activation and/or inhibition affected expression of these signaling molecules. Treatment with 5–125 μM BzATP activated mTOR, as evidenced by 1.4- to 2-fold increased phosphorylation of mTOR, and upregulated HIF1α (by 40% to 150%) and VEGF (by 30% to 70%) protein (Figs. 5*i* and 5*l*). Interestingly, inhibition of P2X7 with A740003 or shP2X7 significantly reduced mTOR activity by 35% or 60% respectively, and downregulated HIF1α and VEGF protein by more than 40%. BzATP stimulation, with P2X7 inhibition, could not obviously increase phosphorylation of mTOR and upregulate HIF1α and VEGF protein (Figs. 5*j*–5*l*). Therefore, P2X7 is involved in angiogenesis and activates the mTOR/HIF1α/VEGF pathway.

P2X7 enhances HOS/MNNG cell growth, metastasis and bone destruction in intra-tibia tumor-bearing mice

To investigate how P2X7 function in osteosarcoma interacted with bone environment, intra-tibia tumor-bearing model was used. HOS/MNNG cells were intra-tibia injected in BALB/c nude/nude mice (n = 6 mice/group). Placebo (phosphate-buffered saline+0.005% dimethyl sulfoxide), BzATP (2.5 mg/kg), A740003 (0.025 mg/kg) or BzATP (2.5 mg/kg) + A740003 (0.025 mg/kg) was administered intraperitoneally every day after the appearance of the tumor mass (day 10 from cell injection) for a total of 20 days. BzATP treatment significantly increased tumor volume by 100%, whereas A740003 reduced tumor size by 50% compared to control and also blocked the pro-growth effect of BzATP (Fig. 6*a*). Tumor differences may be attributed to altered proliferation of tumor cells. Ki67, a maker of cell-cycle progression and proliferation, expression were measured with immunohistochemistry and data showed 70% more nuclear Ki67 in BzATP-treated mice compared to controls. P2X7 receptor inhibition had the opposite effects, reducing Ki67 by more than 45%, on both control and BzATP groups (Fig. 6*b*). Consistent with data from the *in vitro* model, PAS staining of tumor tissues confirmed 35% increased glycogen after mice were treated with BzATP; and more than 40% decreased glycogen was found in A740003 and BzATP +A740003 groups compare to control (Fig. 6*c*). The lung samples were excised from each group of animals and metastasis nodules on the surface of lungs were counted. Our data showed that lung samples from BzATP group had 55% more metastasis nodules than placebo group. While A740003 and BzATP +A740003 treatments reduced the metastasis nodules by 70% and 50% respectively (Fig. 6*d*).

The primary osteosarcoma is capable of developing mixed blastic and lytic destructive lesions in bone. μCT was utilized to access the bone destruction in each group of animals. BzATP group showed significantly more destructive lesions and 12% less of total bone BV/TVs in tibia compared to Placebo group. On the contrary, the destructive lesions were significantly fewer and the total bone BV/TVs were relatively increased after A740003 treatment with or without BzATP (Fig. 6*e*).

P2X7 induces HOS/MNNG cell growth, metastasis and vessel formation in subcutaneous tumor-bearing mice

As supplementary, we also tested tumors derived by subcutaneous injection of human HOS/MNNG cells in BALB/c nude/nude mice (n = 6 mice/group). Placebo, BzATP, A740003 or BzATP+A740003 was administered in the same method as in the intra-tibia model after the appearance of the tumor mass (day 5 from cell injection) for a total of 20 days. BzATP treatment significantly increased tumor volume and weight by 65%, whereas A740003 reduced tumor size and weight by 40% compared to control and also blocked the pro-growth effect of BzATP (Supporting Information Figs. S6A and S6B). 70%–100% more nuclear Ki67 and PCNA were detected in BzATP-treated mice compared to controls. P2X7 receptor

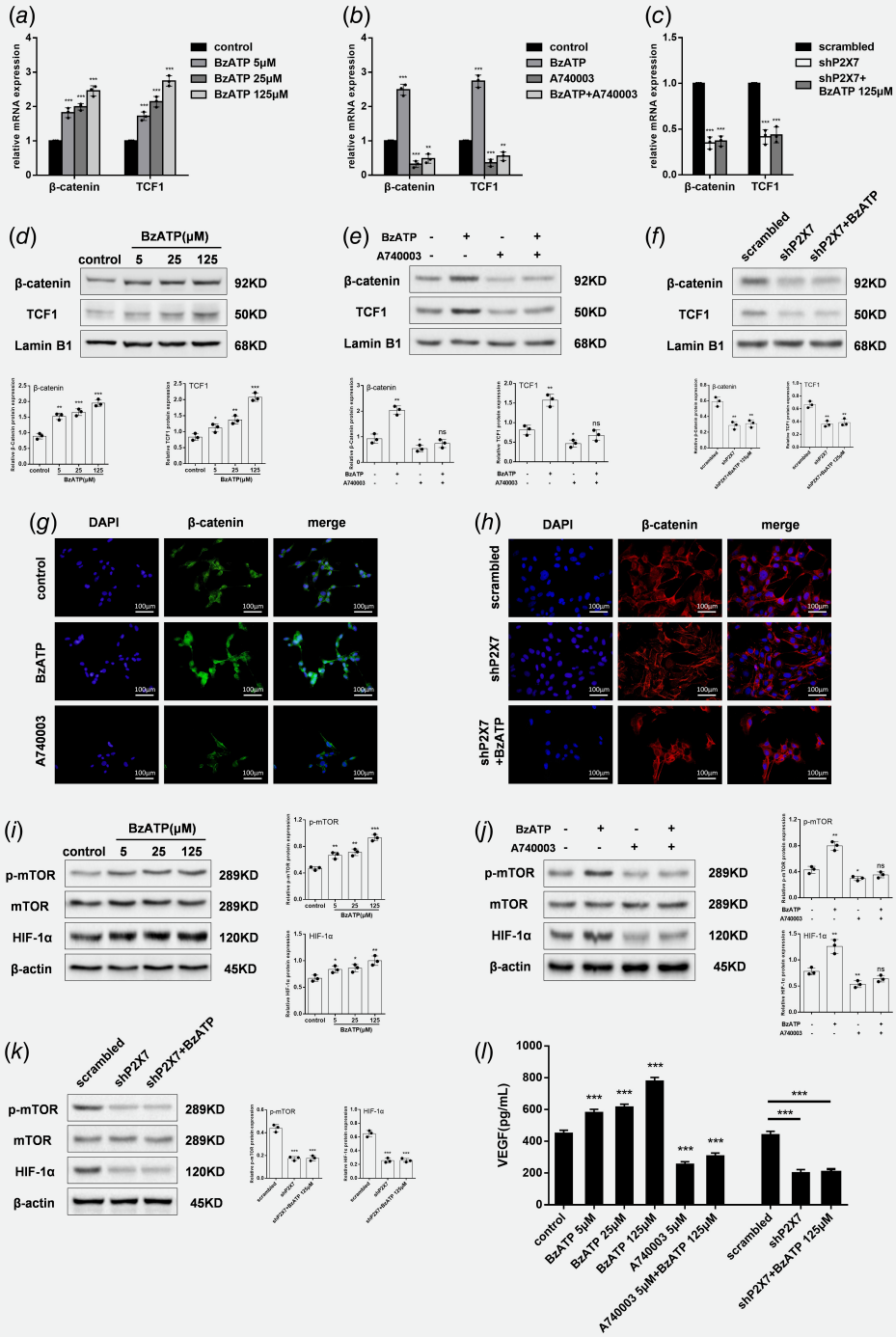

Figure 5. P2X7 activates Wnt/β-catenin and mTOR/HIF1α/VEGF signaling. (*a*) mRNA and (*d*) protein in BzATP-treated (5, 25 or 125 μM for 24 h) HOS/MNNG cells. (*b*) mRNA and (*e*) protein of β-catenin and TCF1, and (*g*) immunofluorescent staining for β-catenin in HOS/MNNG cells treated with BzATP (125 μM) or A740003 (5 μM) for 24 h. (*c*) mRNA and (*f*) protein of β-catenin and TCF1, and (*g*) immunofluorescent staining for β-catenin in HOS/MNNG cells transfected with scrambled or shP2X7 lentiviral vectors or treated with shP2X7 and BzATP (125 μM). Expression of total mTOR, phosphorylated (p)-mTOR (Ser2448) and HIF-1α in HOS/MNNG cells treated with (*i*) BzATP (5, 25 or 125 μM) for 24 h, (*j*) BzATP (125 μM) or A740003 (5 μM) for 24 h, or (*k*) lentiviral vectors or treated with shP2X7 and BzATP (125 μM). (*l*) VEGF protein in HOS/MNNG cells treated with BzATP (5, 25 or 125 μM) or A740003 (5 μM) or both for 24 h, or transfected with lentiviral vectors or treated with shP2X7 and BzATP (125 μM). Relative gene or protein expression was assayed by normalizing with Lamin B1 or β-actin. In Immunofluorescence, secondary antibodies were FITC or Cy3 labeled, and cell nuclei were counterstained with DAPI. VEGF protein was measured using a commercially available human VEGF ELISA kit. Data are means ± SD of 3 independent experiments. $^{***}p < 0.001$, $^{**}p < 0.01$, $^{*}p < 0.05$ *vs.* control. [Color figure can be viewed at wileyonlinelibrary.com]

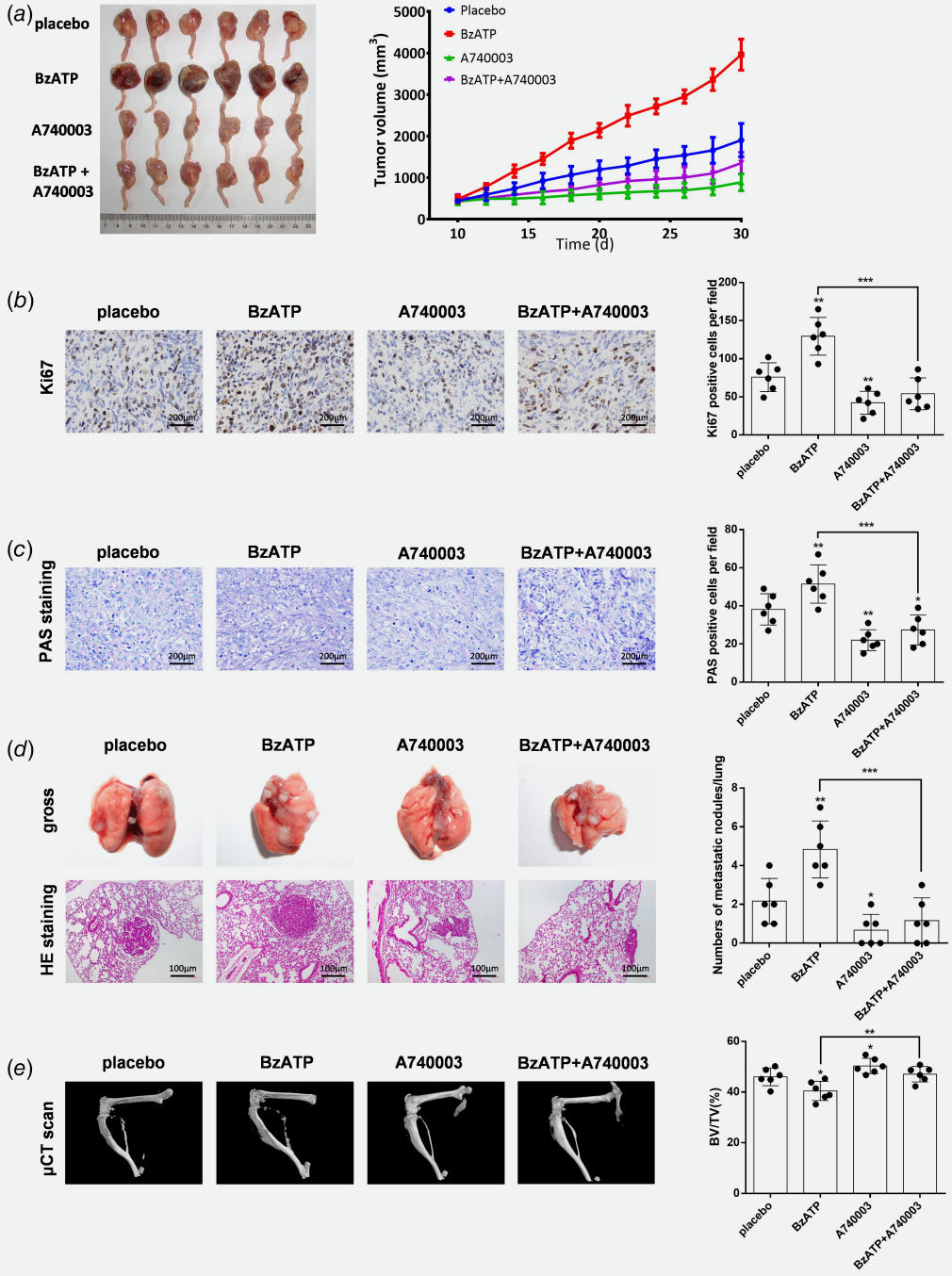

Figure 6. P2X7 induces growth, metastasis and tumor-associated bone destruction of HOS/MNNG cells injected in Balb-c/nude mice. HOS/MNNG cells were resuspended at 1×10^5/10 μl in PBS, and injected into the medullary cavity of the right tibia of mice (n = 24). When tumor volumes reached ~10–100 mm^3 (day 10 from cell injection) mice were divided into 4 groups (n = 6 mice/group), and treated with 200 μl (ip) of placebo (PBS + 0.005% DMSO), BzATP (2.5 mg/kg), A740003 (0.025 mg/kg) or BzATP (2.5 mg/kg) + A740003 (0.025 mg/kg) every 2 days for 20 days. (*a*) Tumor volume measured every 2 days for 20 days. Tumor volume was calculated using the following formula: volume = $\pi/6$ (w1 × (w2)^2), where w1 = major diameter (mm) and w2 = minor diameter (mm) of the tumor. (*b*) Immunohistochemical staining for Ki67 in tumor tissue sections from osteosarcoma-bearing mice. (*c*) PAS staining of tumor tissue for glycogen stores. Ki67 and PAS positive cells were counted using Image Pro Plus 6.0 software. (*d*) Left: Representative images of gross and H&E staining of lung tissue sections from osteosarcoma-bearing mice treated with placebo, BzATP, A740003 or BzATP+A740003. Right: Numbers of metastatic nodules in mice of each treatment groups. (*e*) (left) Representative μCT images and (right) relative volume (BV/TV) of right tibia from osteosarcoma-bearing mice treated with placebo, BzATP, A740003 or BzATP+A740003. BV/TV bone volume/total volume. Data are means ± SD, n = 6 mice/group. $^{***}p < 0.001$, $^{**}p < 0.01$, $^{*}p < 0.05$ *vs.* control. [Color figure can be viewed at wileyonlinelibrary.com]

inhibition reduced Ki67 and PCNA by more than 40%, on both control and BzATP groups (Supporting Information Fig. S6C; Supporting Information Fig. S7A and S7B). PAS staining of tumor tissues confirmed 80% increased glycogen after mice were treated with BzATP; while glycogen decreased more than 30% in A740003 and BzATP+A740003 groups compare to control (Supporting Information Fig. S6D).

H&E staining confirmed that after BzATP treatment 4 of 6 lung samples had lung metastasis but placebo, A740003 or BzATP+A740003 treatment did not result in metastases (Supporting Information Fig. S6E), suggesting that P2X7 increased HOS/MNNG cell metastatic capacity. Additionally, immunohistochemical and immunofluorescent analysis revealed significantly increased Fibronectin in tumor tissues of BzATP-treated mice compared to controls (Supporting Information Fig. S6F; Supporting Information Fig. S7C). In contrast, A740003 or BzATP+A740003 treated mice had less Fibronectin in the tumor tissues, suggesting that P2X7 induced EMT in an *in vivo* osteosarcoma model.

Solid tumor growth depends on adequate vascularization and blood supply.[36] H&E staining of tumor tissues from BzATP-treated mice confirmed twofold or more vascular networks than that of in placebo, A740003 or BzATP+A740003 treated mice (Supporting Information Fig. S6G). Because CD31 is a marker of angiogenesis during tumor growth, we measured marker expression[37] and noted that BzATP treatment increased CD31-positive cells but A740003 or BzATP+A740003 reduced CD31 expression (Supporting Information Fig. S8A and S8B). Therefore, P2X7 stimulated and/or enhanced angiogenesis *in vivo*.

Discussion

The expression and function of P2X7 receptors in osteoblasts is well established,[25,26,38] but less is known about their role in osteosarcoma. We elucidated the molecular mechanisms of P2X7-dependent positive regulation of osteosarcoma cell proliferation, invasion, migration, EMT and angiogenesis. We confirmed that expression of P2X7 was significantly higher in tumor tissues from patients with stage-IV osteosarcoma compared to normal bone tissues. Upregulated P2X7 mRNA and protein expression occurred in 5 different osteosarcoma cell lines, suggesting that P2X7 may be needed for survival and proliferation of osteosarcoma cells. Moreover, P2X7 activation increased plasma membrane permeabilization and intracellular Ca^{2+} in HOS/MNNG cells, indicating that P2X7 is functional in HOS/MNNG cells.

ATP-activated P2X7 receptors are reported to mediate cytotoxic effects in tumor cells.[6] BzATP is a specific P2X7 receptor agonist, showing 5- to 10-fold greater potency than ATP, though it also exhibits activity at other P2 receptors, especially P2X1 and P2X4. However, *in vitro* results showed that BzATP increased proliferation of HOS/MNNG and SAOS-2 cells. In both intra-tibia and subcutaneous osteosarcoma xenograft models, BzATP treatment increased tumor volume and cell proliferation marker (Ki67). These effects were significantly reduced in mice treated with A740003. Thus, P2X7 promotes osteosarcoma cell growth by stimulating cell proliferation. Metastasis or relapse for osteosarcoma patients indicates poor prognosis[2–4] and *in vitro* data showed that P2X7 positively regulates migration and invasion of HOS/MNNG and SAOS-2 cells. In addition, in both *in vivo* models, lung samples from mice treated with BzATP had significantly more chance of metastasis lesions occurrence compared to placebo treated mice, while in intra-tibia model, A740003 and BzATP+A740003 treated mice showed less lung metastasis, suggesting that P2X7 helps to stimulate osteosarcoma growth and metastasis.

Importantly, A740003 reduced both basal and BzATP-stimulated cancer cell growth, migration and invasion to similar levels. Consistently, shRNA silencing P2X7 expression reduced basal cancer cell growth, migration and invasion *in vitro*, and BzATP stimulation could not reverse this inhibitory effect. We also excluded the possibility of the off-target effect of A740003 by confirming that A740003 could not additionally inhibit growth, migration and invasion of P2X7 silenced HOS/MNNG cells. These results are in favor of a participation of P2X7 in the basal cancer cell growth, migration and invasion in the absence of an exogenous stimulus (BzATP). Di Virgilio's group reported relatively high extracellular ATP in tumor microenvironments of experimentally induced tumors, whereas ATP was undetectable in tumor-free healthy tissues. Tumor-derived ATP modulates tumor growth, progression, and the immunosuppressive response.[6,7] So, we presume that the P2X7 receptor is fundamental in osteosarcoma development and is also endogenously stimulated by a basal release of ATP. This will provide an important basis for taking P2X7 blockade as a treatment for osteosarcoma.

The PI3K/Akt signaling cascade plays a critical role in tumor cell growth and bioenergetics, regulating aerobic glycolysis, cell cycle progression and autophagy. Recently, PI3K/Akt has been associated with osteosarcoma progression and resistance to chemotherapeutic drugs.[39–42] BzATP increased Akt activity, but P2X7 receptor inhibition significantly reduced Akt phosphorylation in HOS/MNNG cells. Treatment with a PI3K inhibitor, LY294002, resulted in significantly reduced cell proliferation, migration and invasion. Compared to single-drug administration, treatment with A740003 and a PI3K inhibitor did not cause an additional reduction in cell proliferation, migration and invasion, suggesting that P2X7 promotes tumor growth and metastasis by acting as an upstream regulator of the PI3K/Akt pathway. These results also suggested that the basal growth and metastasis of HOS/MNNG cells can be inhibited through P2X7/PI3K signaling inhibition. So, we presume that the PI3K/Akt pathway is also basally activated by the basal P2X7 activation.

We provide evidence that P2X7 not only modulated the PI3K/Akt pathway, but also its downstream effectors, GSK3β and mTOR/HIF-1α.[41–43] Akt directly phosphorylates GSK-3β at Ser9, which negatively regulates its kinase activity. Here, we report that BzATP treatment caused GSK3β inactivation *in vitro*, whereas P2X7 antagonists or receptor silencing had

the opposite effect on GSK3β activity. GSK3β is a negative regulator of glycogen synthase, driving the consumption of cellular glycogen. Glycogen-rich cells are present in many aggressive tumors, and glycogen is thought to be an important energy source for cancer cells, promoting their survival under conditions of metabolic stress and hypoxia.[35,44–46] We found that untreated HOS/MNNG cells had more glycogen compared to cells with P2X7 receptor blockade or knockdown *in vitro*. In contrast, P2X7 agonist enhanced glycogen accumulation in HOS/MNNG cells *in vitro*. These data were also confirmed *in vivo*, in which A740003-treated osteosarcoma-bearing mice had less tumor glycogen, and BzATP treated animals had increased tumor glycogen. Our data indicate that P2X7 may favor cell survival and progression by inactivating GSK3β and increasing glycogen storage in osteosarcoma cells.

Previous studies indicate that stimulating EMT and increasing CSCs can promote cancer metastasis and relapse.[34,47–50] Cells undergoing EMT are known to acquire stem cell-like properties. Loss of epithelial marker E-cadherin, increased expression of mesenchymal markers Fibronectin and Vimentin and the EMT regulator Snail, which are important events in EMT. We showed that P2X7 activation promoted EMT and stemness, but receptor blockade or silencing suppressed EMT and stemness in HOS/MNNG cells *in vitro*. Wnt signaling has been implicated in EMT-induced CSCs and activated Wnt signaling is said to increase expression of Snail, which inhibits E-cadherin expression to induce EMT.[27] The interaction between the PI3K/Akt and Wnt sigaling through the Akt/GSK3β/β-catenin axis is found to participate in the maintenance of CSC properties and induction of EMT. In the Akt/GSK3β/β-catenin signaling pathway, GSK3β plays an important role in β-catenin phosphorylation and degradation. GSK3β activity can be inhibited by Akt phosphorylation at Ser9 and β-catenin transfers into the nucleus to activate the transcription of downstream target oncogenes including TCF1. Inhibition of GSK3β also increases Snail stability, thus promoting EMT.[28] In this study, P2X7 agonist activated Akt/GSK3β/β-catenin/TCF1 signaling pathways and P2X7 blockade or silencing suppressed these pathways, which resulted in P2X7-dependent EMT inhibition *in vitro*. Thus, we speculate that P2X7 participates in cancer metastasis by partially inducing EMT and osteosarcoma CSCs *via* Akt activation and GSK3β inhibition. These events eventually stimulate the Wnt/β-catenin/TCF1 signaling pathway and enhance the function of Snail.

Angiogenesis is key to tumor progression during which angiogenic proteins such as HIF1α and VEGF act downstream of PI3K/Akt/mTOR signaling pathway.[23,24] We found that BzATP activated mTOR in HOS/MNNG cells and upregulated HIF1α and VEGF downstream factors *in vitro*. P2X7 activation had similar effects on angiogenesis in an *in vivo* subcutaneous osteosarcoma model: BzATP increased expression of endothelial marker CD31 and blood vessel number. Therefore, *in vitro* and *in vivo* results indicate that P2X7 may enhance angiogenesis in osteosarcoma by activating PI3K/Akt/mTOR/HIF1α/VEGF signaling. This P2X7-dependent pro-angiogenic function may be a mechanism leading to P2X7-induced osteosarcoma growth and metastasis.

As osteosarcoma is a tumor arising from the osteogenic matrix, it is characterized by the production of osteoid matrix and immature bone by neoplastic cells. Also, these tumor cells produce many factors that stimulate osteolysis, such as PTHrP, IL-1, IL-6, IL-8, IL-11, and transforming growth factor-β, which induce RANKL expression in osteoblasts or bone marrow stromal cells. Interactions between tumor cells and osteoclasts through these factors can induce the vicious cycle of osteolytic bone destruction, which consists of release of osteolytic mediators by tumor cells, bone degradation, release of growth factors from degraded bone, enhanced tumor cell growth, and further release of osteolytic mediators. In our *in vivo* study, intratibia injection of HOS/MNNG caused mixed blastic and lytic destructive lesions. BzATP significantly increased both blastic and lytic lesions, and decreased bone volumes. While A740007 definitely protected the tumor-beared bone from this bilateral destruction and loss of bone mass, which may suggest that P2X7 activation is prone to induce the osteosarcoma-associated bone destruction through the promoting the proliferation of HOS/MNNG cells, and P2X7 inhibition may be a promising therapy to blockade of the vicious cycle between tumor cell proliferation and bone resorption.

In conclusion, P2X7 was overexpressed in human osteosarcoma tissues and cell lines, and has a vital role in osteosarcoma growth and metastasis. Activation of P2X7 enhanced osteosarcoma cell proliferation, migration and invasion, induced EMT, increased cell stemness, augmented VEGF release and angiogenesis and induced the osteosarcoma-associated bone destruction. These functions of P2X7 are partially mediated by activation of PI3K/Akt/GSK3β/β-catenin and/or mTOR/HIF1α/VEGF signaling pathways. However, more work is required to characterize mechanisms of P2X7 endogenously activation and by which P2X7 functions at protein and RNAs. We offer initial evidence that P2X7 is a potential therapeutic target, and that targeted inhibition of P2X7 may be useful for treating metastatic osteosarcoma.

Acknowledgements

This study was supported by the National Natural Science Foundation of China (Grant nos. 51537004, 81301552 and 51807078).

References

1. Hayden JB, Hoang BH. Osteosarcoma: basic science and clinical implications. *Orthop Clin North Am* 2006;37:1–7.
2. Bielack SS, Kempf-Bielack B, Delling G, et al. Prognostic factors in high-grade osteosarcoma of the extremities or trunk: an analysis of 1,702 patients treated on neoadjuvant cooperative osteosarcoma study group protocols. *J Clin Oncol* 2002; 20:776–90.

3. Chou AJ, Geller DS, Gorlick R. Therapy for osteosarcoma: where do we go from here? *Paediatr Drugs* 2008;10:315–27.
4. Link MP, Goorin AM, Miser AW, et al. The effect of adjuvant chemotherapy on relapse-free survival in patients with osteosarcoma of the extremity. *N Engl J Med* 1986;314:1600–6.
5. Pellegatti P, Raffaghello L, Bianchi G, et al. Increased level of extracellular ATP at tumor sites: in vivo imaging with plasma membrane luciferase. *PloS one* 2008;3:e2599.
6. Burnstock G, Di Virgilio F. Purinergic signalling and cancer. *Puriner Signal* 2013;9:491–540.
7. Di Virgilio F. Purines, purinergic receptors, and cancer. *Cancer Res* 2012;72:5441–7.
8. Giuliani AL, Colognesi D, Ricco T, et al. Trophic activity of human P2X7 receptor isoforms a and B in osteosarcoma. *PloS one* 2014;9:e107224.
9. Giannuzzo A, Pedersen SF, Novak I. The P2X7 receptor regulates cell survival, migration and invasion of pancreatic ductal adenocarcinoma cells. *Mol Cancer* 2015;14:203.
10. Adinolfi E, Raffaghello L, Giuliani AL, et al. Expression of P2X7 receptor increases in vivo tumor growth. *Cancer Res* 2012;72:2957–69.
11. Amoroso F, Capece M, Rotondo A, et al. The P2X7 receptor is a key modulator of the PI3K/GSK3beta/VEGF signaling network: evidence in experimental neuroblastoma. *Oncogene* 2015;34:5240–51.
12. Yadav M, Singh A, Rizvi N, et al. The role of P2X7R purinoreceptor in osteosarcoma. *Adv Mod Oncol Res* 2015;1:88–96.
13. Baricordi OR, Melchiorri L, Adinolfi E, et al. Increased proliferation rate of lymphoid cells transfected with the P2X(7) ATP receptor. *J Biol Chem* 1999;274:33206–8.
14. Adinolfi E, Callegari MG, Ferrari D, et al. Basal activation of the P2X7 ATP receptor elevates mitochondrial calcium and potential, increases cellular ATP levels, and promotes serum-independent growth. *Mol Biol Cell* 2005;16:3260–72.
15. Amoroso F, Falzoni S, Adinolfi E, et al. The P2X7 receptor is a key modulator of aerobic glycolysis. *Cell Death Dis* 2012;3:e370.
16. Jelassi B, Chantome A, Alcaraz-Perez F, et al. P2X(7) receptor activation enhances SK3 channels- and cystein cathepsin-dependent cancer cells invasiveness. *Oncogene* 2011;30:2108–22.
17. Adinolfi E, Cirillo M, Woltersdorf R, et al. Trophic activity of a naturally occurring truncated isoform of the P2X7 receptor. *FASEB J* 2010;24:3393–404.
18. Besson P, Driffort V, Bon E, et al. How do voltage-gated sodium channels enhance migration and invasiveness in cancer cells? *Biochim Biophys Acta* 2015;1848:2493–501.
19. Di Virgilio F, Adinolfi E. Extracellular purines, purinergic receptors and tumor growth. *Oncogene* 2017;36:293–303.
20. Giannuzzo A, Saccomano M, Napp J, et al. Targeting of the P2X7 receptor in pancreatic cancer and stellate cells. *Int J Cancer* 2016;139:2540–52.
21. Park YL, Kim HP, Cho YW, et al. Activation of WNT/beta-catenin signaling results in resistance to a dual PI3K/mTOR inhibitor in colorectal cancer cells harboring PIK3CA mutations. *Int J Cancer* 2019;144:389–401.
22. Politz O, Siegel F, Barfacker L, et al. BAY 1125976, a selective allosteric AKT1/2 inhibitor, exhibits high efficacy on AKT signaling-dependent tumor growth in mouse models. *Int J Cancer* 2017;140:449–59.
23. Chen QY, Jiao DM, Wu YQ, et al. MiR-206 inhibits HGF-induced epithelial-mesenchymal transition and angiogenesis in non-small cell lung cancer via c-met /PI3k/Akt/mTOR pathway. *Oncotarget* 2016;7:18247–61.
24. Granville CA, Memmott RM, Gills JJ, et al. Handicapping the race to develop inhibitors of the phosphoinositide 3-kinase/Akt/mammalian target of rapamycin pathway. *Clin Cancer Res* 2006;12:679–89.
25. Grol MW, Brooks PJ, Pereverzev A, et al. P2X7 nucleotide receptor signaling potentiates the Wnt/beta-catenin pathway in cells of the osteoblast lineage. *Purinergic Signal* 2016;12:509–20.
26. Alqallaf SM, Evans BA, Kidd EJ. Atypical P2X receptor pharmacology in two human osteoblast-like cell lines. *Br J Pharmacol* 2009;156:1124–35.
27. Stemmer V, de Craene B, Berx G, et al. Snail promotes Wnt target gene expression and interacts with beta-catenin. *Oncogene* 2008;27:5075–80.
28. Zhou BP, Deng J, Xia W, et al. Dual regulation of snail by GSK-3beta-mediated phosphorylation in control of epithelial-mesenchymal transition. *Nat Cell Biol* 2004;6:931–40.
29. Lamouille S, Xu J, Derynck R. Molecular mechanisms of epithelial-mesenchymal transition. *Nat Rev Mol Cell Biol* 2014;15:178–96.
30. Gupta GP, Massague J. Cancer metastasis: building a framework. *Cell* 2006;127:679–95.
31. Lin X, Chen W, Wei F, et al. POMC maintains tumor-initiating properties of tumor tissue-derived long-term-cultured breast cancer stem cells. *Int J Cancer* 2017;140:2517–25.
32. Ge Y, Weygant N, Qu D, et al. Alternative splice variants of DCLK1 mark cancer stem cells, promote self-renewal and drug-resistance, and can be targeted to inhibit tumorigenesis in kidney cancer. *Int J Cancer* 2018;143:1162–75.
33. Hufbauer M, Maltseva M, Meinrath J, et al. HPV16 increases the number of migratory cancer stem cells and modulates their miRNA expression profile in oropharyngeal cancer. *Int J Cancer* 2018;143:1426–39.
34. Chen HJ, Huang RL, Liew PL, et al. GATA3 as a master regulator and therapeutic target in ovarian high-grade serous carcinoma stem cells. *Int J Cancer* 2018;143:3106–19.
35. Favaro E, Bensaad K, Chong MG, et al. Glucose utilization via glycogen phosphorylase sustains proliferation and prevents premature senescence in cancer cells. *Cell Metab* 2012;16:751–64.
36. Neufeld G, Kessler O. Pro-angiogenic cytokines and their role in tumor angiogenesis. *Cancer Metastasis Rev* 2006;25:373–85.
37. Nefedova NA, Kharlova OA, Danilova NV, et al. Markers of angiogenesis in tumor growth. *Arkh Patol* 2016;78:55–62.
38. Gartland A, Hipskind RA, Gallagher JA, et al. Expression of a P2X7 receptor by a subpopulation of human osteoblasts. *J Bone Mineral Res* 2001;16:846–56.
39. Ma L, Fu Q, Xu B, et al. Breast cancer-associated mitochondrial DNA haplogroup promotes neoplastic growth via ROS-mediated AKT activation. *Int J Cancer* 2018;142:1786–96.
40. Zhang J, Yu XH, Yan YG, et al. PI3K/Akt signaling in osteosarcoma. *Clin Chim Acta* 2015;444:182–92.
41. Fruman DA, Rommel C. PI3K and cancer: lessons, challenges and opportunities. *Nat Rev Drug Discov* 2014;13:140–56.
42. Wang C, Gu C, Jeong KJ, et al. YAP/TAZ-mediated Upregulation of GAB2 leads to increased sensitivity to growth factor-induced activation of the PI3K pathway. *Cancer Res* 2017;77:1637–48.
43. Yu J, Wang X, Lu Q, et al. Extracellular 5′-nucleotidase (CD73) promotes human breast cancer cells growth through AKT/GSK-3beta/beta-catenin/cyclinD1 signaling pathway. *Int J Cancer* 2018;142:959–67.
44. Cheng KW, Agarwal R, Mitra S, et al. Rab25 increases cellular ATP and glycogen stores protecting cancer cells from bioenergetic stress. *EMBO Mol Med* 2012;4:125–41.
45. Witney TH, Carroll L, Alam IS, et al. A novel radiotracer to image glycogen metabolism in tumors by positron emission tomography. *Cancer Res* 2014;74:1319–28.
46. Zubair H, Azim S, Srivastava SK, et al. Glucose metabolism reprogrammed by overexpression of IKKepsilon promotes pancreatic tumor growth. *Cancer Res* 2016;76:7254–64.
47. Roseweir AK, Kong CY, Park JH, et al. A novel tumor-based epithelial-to-mesenchymal transition score that associates with prognosis and metastasis in patients with stage II/III colorectal cancer. *Int J Cancer* 2019;144:150–9.
48. Wu W, Chen F, Cui X, et al. LncRNA NKILA suppresses TGF-beta-induced epithelial-mesenchymal transition by blocking NF-kappaB signaling in breast cancer. *Int J Cancer* 2018;143:2213–24.
49. Shen Y, Zhang W, Liu J, et al. Therapeutic activity of DCC-2036, a novel tyrosine kinase inhibitor, against triple-negative breast cancer patient-derived xenografts by targeting AXL/MET. *Int J Cancer* 2019;144:651–64.
50. Oh E, Kim YJ, An H, et al. Flubendazole elicits anti-metastatic effects in triple-negative breast cancer via STAT3 inhibition. *Int J Cancer* 2018;143:1978–93.